Trans. Magn. Soc. Japan, 4, 28–33 (2004)

Finite-Element Capacitance Calculation and Spin-dependent Transport Modeling of Double Magnetic Tunnel Junctions

M.B.A. Jalil[1], C. W. Kim[1], Y. Takemura[2], and J. Shirakashi[3]
[1]National University of Singapore, *10 Kent Ridge Crescent, Singapore 117576*
[2] Yokohama National University, *79-5 Tokiwadai, Hodogaya, Yokohama, 240-8501, Japan*
[3] Akita Prefectural University, *84-4 Ebinokuchi, Tsuchiya, Honjo, Akita, 015-0055, Japan*

We model the combined effects of Coulomb blockade (CB) and spin-dependent tunneling in a nanoscale planar-type Ni/NiO double-junction, based on the geometry of a proposed experimental structure. Rectangular and disk-shaped island electrodes, of a size range of w =10 to 50 nm are considered. Precise determination of the circuit capacitances is performed using finite-element (FE) methods. The calculated capacitance values differ significantly from those obtained using analytical formulae. For instance, the island self-capacitance C_s values are about five times larger, which means that the operational temperature for the CB device is seriously over-estimated by the analytical formulae. The capacitance calculations also show that an extended gate covering both the island and the contact electrodes, can improve the gate sensitivity by 95% with only a minimal increase (0.3%) of the self-capacitance C_s. This avoids the need for an ultrasmall gate lithographed exactly below the island in the double junction device. The tunneling current is then obtained using the calculated capacitance values, and incorporates both single tunneling and cotunneling. Finally, we present the temperature dependence of the I-V and I-V_g characteristics and TMR values which, being based on actual fabricated dimensions, will be significant for comparison with experimental results.

Key words: magnetic tunnel junction, single electron tunneling, Coulomb blockade, tunneling magneto-resistance, nano structure, capacitance calculation.

1. Introduction

A double-junction device consisting of a nanometer-sized "island" electrode, coupled to ferromagnetic (FM) contact electrodes across thin tunnel barriers, shows a combination of tunneling magnetoresistive (TMR)[1] and Coulomb blockade (CB) effects.[2] The TMR effect arises from the differential density of states and transmission coefficient for majority and minority spin carriers across the tunnel barrier. The CB effect becomes significant when the electrostatic charging energy $E_c = e^2/2C$ due to a discrete charge e exceeds thermal energy k_BT, and the tunnel resistance R_t is much larger than the resistance quantum.[2] Under these conditions, current is suppressed below a certain threshold voltage V_t, while correlated sequential tunneling occurs at bias $V > V_t$. With the inclusion of a gate electrode, we can adjust the island potential and control the discrete charge tunneling, thus forming a single electron transistor (SET).[3]

In a SET with ferromagnetic (FM) junctions,[4,5] an extra degree of control exists since the tunneling current can be modulated by changing the relative alignment of island and contact magnetizations, by means of an external magnetic field. In addition, the combination of TMR and CB effects in FM-SETs has led to novel phenomena such as magneto-Coulombic oscillations[6] due to Zeeman splitting and bias modulation of TMR.[7,8] More significantly from the viewpoint of magnetic storage applications is the enhancement of TMR due to higher-order cotunneling effects.[9,10]

There are two possible practical realizations of metallic FM-SETs i.e. either in granular[11,12] form or planar junction geometry.[13] The former has the advantage of achieving very small island sizes and hence enhanced operational temperature without the need for lithography of individual islands. On the other hand, there is no precise control on the mean size and placement of the islands, thus resulting in a wide variability in critical parameters such as the threshold voltage. By contrast, a precise control of junction thickness and island size is achievable in the planar junction geometry. Shirakashi *et al.* [14] achieved the controlled fabrication of the double tunnel barrier of a Nb/NbO SET by means a scanning probe microscope. This work was extended to oxidation on a smaller scale using an atomic force microscope (AFM).[15] Using this technique, island size of w < 100 nm can be realized.

With such a degree of precision in the fabrication, one may obtain rectangular islands with almost uniform barrier thickness. In view of the near-ideal geometry, it may seem justifiable to use analytical capacitance formulae to estimate the junction, gate and island self-capacitances. In this paper, we calculate the capacitive couplings of a double-junction circuit, based on an experimental structure, by finite element methods. Our calculated values reveal large discrepancies compared to the analytical formulae. This is due to the assumptions inherent in the analytical formulae, (e.g. infinitely long tunnel junctions, and complete electrostatic isolation of the island), which are not valid in a nanoscale double-junction device. The need for precise determination of the capacitances in a SET is necessary since important quantities such as the Coulomb gap, operational temperature and period of gate oscillations are strongly influenced by the capacitance values. Based on the precise capacitance values, we obtain the I-V and I-V_g characteristics of the SET. The single tunneling and cotunneling rates are calculated using the orthodox theory in the global rule limit[16,17] and second order

perturbation result,[18] respectively. The average current is then obtained using the Master Equation. Finally, the modulation of the TMR with both V and V_g due to the difference in the relative contribution of single and cotunneling is demonstrated.

2. Model

The capacitance matrix of the system is computed based on a typical planar Ni/NiO/Ni double junction experimental structure.[15] The capacitance calculations are performed by 3D finite element method using a software package called Fastcap.[19] It is necessary to first generate a neutral file for each electrode shape to store the geometric and meshing information. The neutral files of rectangular electrodes can be generated by Fastcap itself, while electrodes with curved surfaces (e.g. disk-shaped islands), have to be drawn and meshed in a commercial finite-element software (e.g. Partran) before being exported as a neutral file into Fastcap. In the meshing of rectangular electrodes, the surface mesh cell is made 10 times finer at the edges, where charge distribution varies most rapidly. The mesh cell dimension for the disk-shaped island is set at 0.15 of its radius, which gives rise to ~ 600 elements per island. Fig. 1 shows the meshed electrodes of a double-junction system with a disk-shaped island for three geometries – no gate, restricted and extended gates. The thickness t of the electrodes and gate-island d_g and contact-island d_j spacings are kept constant at 10 nm, 2 nm and 10 nm, respectively. The island size w is varied while keeping the ratio l/w = 10, where l is the length of the contact electrodes. The calculations are also repeated for all three geometries for rectangular islands. Based on an input file listing the relative position of each electrode in

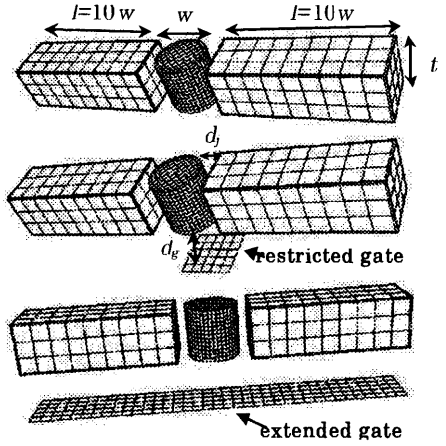

Fig. 1. Finite-element meshed model of actual experimental structure. Two island shapes, disk and rectangular (not shown), are modeled for size w ranging from 10 to 50 nm. We also consider three gate geometries, i.e. no gate (top), restricted gate (middle) and extended gate (bottom). Other parameters: length of contacts l = 10w, barrier thickness d_j = 2 nm, gate separation d_g = 10 nm.

3-D space, Fastcap calculates the capacitive coupling between each pair of mesh elements using a known multipole technique.[20] These inter-element couplings are then summed to yield the self- and cross-capacitances of whole electrodes in the circuit, which are collectively grouped together as a capacitance matrix **C**.

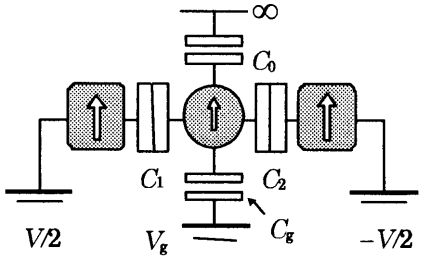

Fig. 2. Schematic diagram of a double-junction circuit. V is the source-drain bias across the two contact electrodes while V_g is the bias applied to the back-gate plane. C_0 is the stray capacitance due to field lines which escape out to an imaginary ground at infinity. Arrows indicate the island and contact magnetization. When the island magnetization reverses, we obtain a switch between parallel (p) and antiparallel (a) alignments.

From the **C** matrix, we can extract the values of $C_{1,2}$, C_g and C_0 which correspond to the (left/right) junction, gate and stray capacitances, respectively, as shown in the schematic diagram of a SET circuit (Fig. 2). We then apply Kirchhoff's equations to solve for the potential on the island electrode as a function of the number of discrete island charges n. These yield

$$\phi(n) = \frac{(C_1 - C_2)V + C_g V_g + 2ne}{C_s}, \qquad (1)$$

where $C_s = C_1 + C_2 + C_g + C_0$ is the total or self-capacitance of the island. The free energy change due to a tunneling event ("tunneling energy") is given by the total capacitive energy E_c less the work done W by the external bias sources due to the displacement of charges (both discrete tunneling and continuous polarization charges) at the contact electrodes. The tunneling energy across the left/right junctions in either direction are:

$$\Delta E_1^{\sigma}(n) = \frac{e}{C_s}\left[e/2 + \sigma\left(ne - C_2 V + C_g V_g - (C_g + C_0)V/2\right)\right],$$
$$\Delta E_2^{\sigma}(n) = -\frac{e}{C_s}\left[-e/2 + \sigma\left(ne + C_1 V + C_g V_g + (C_g + C_0)V/2\right)\right], \qquad (2)$$

where $\sigma = \pm 1$ denotes forward(+)/reverse(−) direction with reference to the field gradient. A positive ΔE means that the Fermi level within the island is shifted above that of the source electrode due to single charging energy. By applying the orthodox theory,[17] which is applicable to metallic SET circuits considered here, the tunneling rate is given by

$$\Gamma_i^{\sigma}(n) = \frac{-\Delta E_i^{\sigma}(n)}{e^2 R_{ti}\left[1-\exp\left(\Delta E_i^{\sigma}(n)/k_B T\right)\right]}, \quad (3)$$

where i is the junction index, and R_{ti} the tunneling resistance. The spin-dependent effect in Eq. (3) arises from the dependence of R_{ti} on the relative alignment of the junction magnetizations, following Julliere's model.[21] For the extreme case of either full parallel/antiparallel alignments, we have

$$R_t = 2R_0/(1+\alpha P_l P_r), \quad (4)$$

where α = 1 (−1) applies for (anti-)parallel alignment, and $P_{l,r}$ is the spin polarization of the left/right junctions. Our model assumes complete spin relaxation of the tunneling electron to the equilibrium spin polarization value of the junction electrode it is residing in. Thus, Γ_i^{σ} in Eq. (3) is independent of the electron spin. For the cotunneling rate, we use the equation from second-order perturbation theory[18] with lifetime broadening to remove the singularities which arise at resonant values of the virtual intermediate state energies,[9,22] i.e.

$$\Lambda^{\sigma}(n) = \frac{\hbar}{8\pi e^4}\left(\frac{1}{R_{t1}\times R_{t2}}\right)\int_{-\infty}^{\infty}\frac{\varepsilon(\varepsilon-\sigma eV)\exp(\sigma eV/2T)}{\sinh(\varepsilon/2T)\sinh[(\varepsilon-\sigma eV)/2T]}\times f(\varepsilon,\sigma)d\varepsilon. \quad (5)$$

The function $f(\varepsilon,\sigma)$ is the coherent sum of two cotunneling "channels" (the virtual state may be a transient electron or hole on the island). This is given by

$$f(\varepsilon,\sigma) = \left|\frac{1}{\varepsilon+\Delta E_1^{\sigma}(n)+i\gamma^{\sigma}} + \frac{1}{-\varepsilon+\Delta E_2^{\sigma}(n)+\sigma eV+i\gamma^{\sigma}}\right|^2, \quad (6)$$

where $\gamma$is the inverse of the virtual intermediate state lifetime, as given by Eq. (4) of Ref. 9. A finite γavoids the divergence of the integral in Eq. (5), which occurs if the virtual state falls within a forbidden energy range between the initial and final energies.[23]

The average current is obtained using the Master equation (ME) method. The ME consists of a set of linear equations, representing the total rate connecting each state with its neighbors. Upon solving these equations one obtains the steady state probability p_n of a state having n island charges. For the double-junction system, with just a single island, the ME is particularly simple because (a) only single tunneling rates Γ_i^{σ} need to be considered, and (b) all transitions occur between nearest-neighbor ($n \rightarrow n\pm1$). Λ^{σ} is not included in the ME because a cotunneling process, in transferring a charge across both junctions, will not result in any change in the number of island charges. (Λ^{σ} will however be involved in determining the steady-state current). Due to factor (b), the ME reduces to a linear birth-death equation which can be readily solved by a recursive product:[17,24]

$$p_n = p_{n-1}\frac{\Gamma_{n-1,n}}{\Gamma_{n,n-1}} \Rightarrow p_n = p_0\prod_{k=0}^{n-1}\frac{\Gamma_{k,k+1}}{\Gamma_{k+1,k}}, \quad (7)$$

where $\Gamma_{i,j}$ is the transition rate between states i and j. $\Gamma_{i,j}$ is non-zero only between nearest neighboring states, and is related to $\Gamma_i^{\sigma}(n)$ of Eq. (3) as follows

$$\begin{aligned}\Gamma_{n,n+1} &= \Gamma_1^{+}(n)+\Gamma_2^{-}(n),\\ \Gamma_{n,n-1} &= \Gamma_1^{-}(n)+\Gamma_2^{+}(n).\end{aligned} \quad (8)$$

Note that our assumption of instantaneous spin relaxation leads to zero spin accumulation on the island, and zero spin-split in the Fermi energy. Thus, the state probability p_n and transition rate $\Gamma_{i,j}$ will be dependent only on the total number of island charges n, but not the spins of these charges, unlike in Ref. 25.

The average current is subsequently obtained as the total tunneling rate (single and cotunneling rates) weighted by the state probability i.e.,

$$I = e\sum_{n,\sigma} p_n\sigma\times\Lambda^{\sigma}(n). \quad (9)$$

Note that $\Lambda^{\sigma}(n)$ contains *both* the single and cotunneling contributions, as can be seen from Eq. (6) of Ref. 9. Finally, TMR is defined as the fractional change in current between the parallel and antiparallel alignments of the double junction magnetizations.

3. Results and Discussions

The junction $C_{1,2}$, gate C_g and island self-capacitances C_s of a double-junction system with rectangular island are plotted as a function of island size w over a range of 10 to 50 nm [Fig. 3(a) to (c)]. For comparison, we also plot the analytical estimates, based on simple planar junction and isolated sphere geometry, i.e.

$$\begin{aligned}(C_{1,2})_{\text{est}} &= \varepsilon_0\varepsilon_r A_j/d_j,\\ (C_g)_{\text{est}} &= \varepsilon_0\varepsilon_r A_g/d_g,\\ (C_s)_{\text{est}} &= 4\pi\varepsilon_0\varepsilon_r R_{eq}.\end{aligned} \quad (10)$$

A_j (A_g) is the area of overlap between the island and contact (gate) electrodes and d_j and d_g the distance between the electrodes. R_{eq} is the equivalent radius of a sphere which gives the same volume as the rectangular island electrode, i.e. $4\pi R_{eq}^3/3 = w^2 t$. The dielectric constant ε_r for NiO is taken to be 9.8. For the no-gate geometry, the actual $C_{1,2}$ is almost twice the analytical estimate [Fig. 3(a)]. The discrepancy is due to the significant coupling between the top, bottom, front and back surfaces of the two junction electrodes, given the shape of the junction electrodes. These couplings are neglected by the analytical model, which assumes a pair of (two-dimensional) plate electrodes. The discrepancy is slightly reduced when gate electrodes are present since part of the coupling between the bottom surfaces

of the island and contact electrodes is diverted to the gate electrode instead. For the gate capacitances C_g [Fig. 3(b)], the analytical estimate is reasonably good (within 10%) compared to the restricted gate case. The discrepancy is smaller because coupling between the gate plane and the island electrode surfaces other than its bottom surface is diminished by the larger gate separation distance. Furthermore, due to the position of the gate, only the lower parts of these surfaces are significantly coupled to the gate. The largest discrepancy of up to a factor of 5 exists between the analytical and numerical values of the self-capacitance C_s [Fig. 3(c)]. For example, in the case of w = 50 nm with a restricted gate, C_s = 97.4 aF, but $(C_s)_{est}$ is only 21.7 aF. The analytical formula assumes an isolated charged sphere, i.e. it considers only the stray field lines which extend to infinity. In the actual experimental set-up, this stray contribution C_0 is only a minor contributor to C_s. The bulk of C_s is accounted for by $(C_1 + C_2)$ due to the strong coupling between the island and contact electrodes across the very thin tunneling barrier (d_j = 2 nm), while the coupling C_g to the gate plane also accounts for a significant fraction. With a restricted gate geometry and w = 50 nm, C_0 accounts for only 5% of C_s. The large difference between C_s and $(C_s)_{est}$ has a practical implication since C_s sets the maximum temperature T_0 at which effective Coulomb blockade effect occurs (i.e. $k_B T_0 < e^2/C_s$). Since C_0 plays such an insignificant role, we can do much better in our analytical estimate by taking the self-capacitance as the sum of junction and gate capacitances, i.e.

$$(C_s)'_{est} = (C_1)_{est} + (C_2)_{est} + (C_g)_{est} = \varepsilon_0 \varepsilon_r (2A_j/d_j + A_g/d_g), \quad (11)$$

although there is a still a discrepancy of ~ 50%, as shown in Fig. 3(c). Note that the calculated C_s is virtually unchanged (< 0.3%) when the gate plane is extended to cover the island and both contact electrodes. However, C_g which is a measure of the gate sensitivity of the device is significantly enhanced by extending the gate dimension, especially for the smallest island size w. For instance, for w = 10 nm, the increase in C_g is almost two-fold from 1.02 aF to 1.98 aF, while the fractional change in C_s is much smaller, from 18.10 aF to 18.17 aF. The practical implication is that, for the back-gate geometry considered here, using an extended gate confers the twin advantages of easier fabrication and greater gate sensitivity, at virtually no cost in the increase of C_s and consequent lowering of the operational temperature.

Based on the calculated capacitance values and considering single tunneling process only, the I-V and I-V_g characteristics are obtained at different temperatures T. Fig. 4(a) is the I-V characteristic for the specific case of a double junction with a restricted gate, having dimensions w = 10 nm, d_j = 2 nm, d_g = 10 nm and l = 10w. The value of T ranges from 0.001 to $3T_0 = e^2/k_B C_s$, where T_0 = 101.6 K corresponding to C_s = 18.2 aF, while V_g is set at 0V. The Coulomb gap occurs for voltage range $|V| < e/C_s$ = 8.8 mV. The blockade begins to be thermally smeared at T = 0.1 T_0 = 10.2 K and becomes indistinct at 0.3 T_0 = 30.5 K. The I-V_g [Fig 4(b)] is obtained at source-drain V = 0.5 e/C_s = 4.4 mV where the amplitude of the gate oscillation is largest. The period of oscillation is e/C_g = 80.8 mV, corresponding to

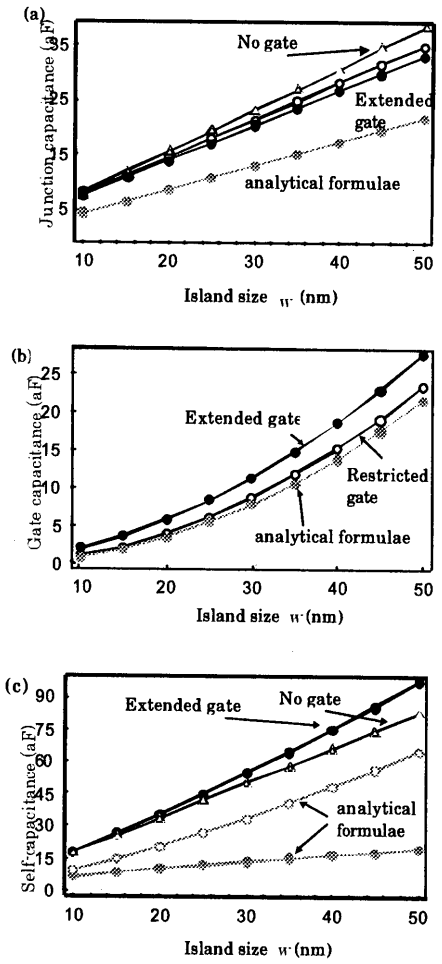

Fig. 3. Precise values of (a) junction C_j, (b) gate C_g and (c) self C_s as a function of island size w. Triangular, open-circle and filled-circle plot symbols denote no-gate, restricted gate and extended gate geometries, respectively. Gray curves with filled-circle symbols denote analytical formulae in Eq. (10), while the gray curve with open-circle symbols in (c) indicates the alternative formula given in Eq. (11).

C_g = 1.98 aF. The oscillation progressively disappears as T is raised above 0.1 T_0 = 10.2 K and totally disappears at 0.5T_0 = 50.8 K. Thus, based on the calculated capacitance values, we find that a sub-liquid N_2 temperature is still required to observe features of single electron tunneling even for the smallest island size considered.

For a symmetric Ni-Ni island-Ni double junction, there is no bias modulation of TMR if we assume the Julliere model of spin-dependent tunneling and restrict ourselves to first-order tunneling.[4] We now include the contribution of second-order tunneling or cotunneling. Figs. 5(a) and (b) plot the resulting I-V characteristic and the corresponding TMR, which is defined as

$$\mathrm{TMR} = \frac{I_p - I_a}{I_a}, \tag{12}$$

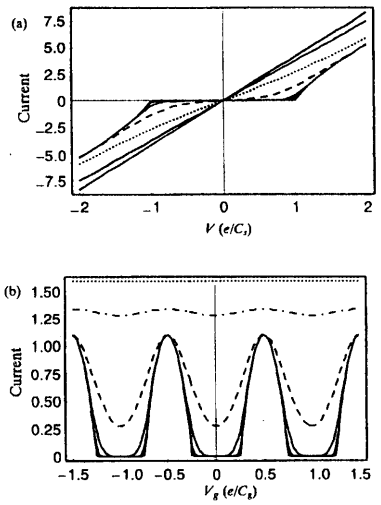

Fig. 4(a) Current versus source-drain voltage (I-V) characteristic based on precise capacitance values for the case of rectangular island of size w = 10 nm, at V_g = 0 V and temperatures T/T_0 = 10^{-3}, 3×10^{-3}, 10^{-2}, 3×10^{-2}, 0.1 (dashed), 0.3 (dotted), 1 and 3. (b) Current versus gate voltage (I-V_g) characteristic for the same structure at T/T_0 = 10^{-3}, 3×10^{-3}, 10^{-2}, 3×10^{-2}, 0.1 (dashed), 0.3 (dash-dot), and 0.5 (dotted).

where $I_{a,p}$ is the current flow when the island and contact magnetizations are parallel (p) or antiparallel (a) to each other. The tunnel resistances of each Ni-NiO-Ni junction for the two magnetization alignments are

$$R_t^{(p)} = R_0/(1+P_{\mathrm{Ni}}^2),$$
$$R_t^{(ap)} = R_0/(1-P_{\mathrm{Ni}}^2), \tag{13}$$

where for simplicity R_0 = 1 Ω and the spin polarization of Ni P_{Ni} = 23%.[26] The I-V curves [Fig. 5(a)] are plotted for T = 0.01 T_0 to 0.2 T_0 (1.0 to 20.4 K). As we have seen in Fig 4(a), the Coulomb gap becomes indistinct beyond $0.1T_0$. An important difference is that in the presence of cotunneling, the sharp Coulomb gap profile which exists for $T \leq T_0/100$ in Fig. 4(a) has been smoothened out. Comparing the I-V and TMR curves, we find that at $V >> V_t = e/C_s$ = 8.8 mV, where single tunneling predominates, the TMR reaches an asymptotic value of 11.2%. This agrees with the theoretical value of $2P_{\mathrm{Ni}}^2/(1-P_{\mathrm{Ni}}^2)$ obtained from the Julliere's model. As V falls below V_t, the TMR rises sharply as the contribution from cotunneling becomes significant, and at the lowest V, TMR reaches up to 22.9%, which is close to the prediction of $[1+2P_{\mathrm{Ni}}^2/(1-P_{\mathrm{Ni}}^2)]^2-1$ obtained from Takahashi and Maekawa's model.[9] The I-V_g [Fig. 6(a)] shows a similar inverse relation between current and TMR [Fig. 6(b)] values. At $V_g = (n+1)e/2C_g$ = $(n+1)$ 40.4 mV, the CB is lifted. This results in a current peak, but TMR drops to 11.2%. Conversely at $V_g = ne/2C_g$, we are in deep CB region, which results in a low current dominated by cotunneling, resulting in a high TMR of 22.9%. It is interesting to note that the modulation of TMR is much more sensitive to T since it relies on the interplay between cotunneling and single tunneling.

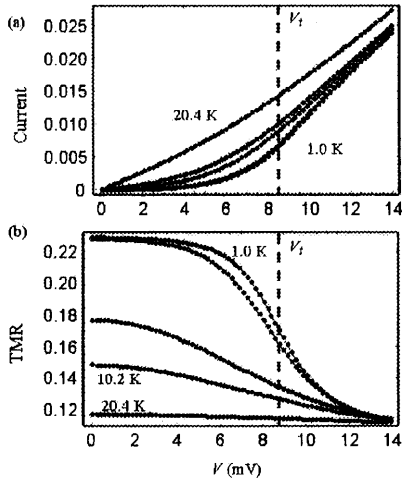

Fig. 5. (a) I-V characteristics and (b) TMR based on the same structure as in Fig. 4 for T/T_0 = 0.01 (= 1.0 K), 0.02, 0.03, 0.075, 0.1 and 0.2 (= 20.4 K). V_t denotes the threshold voltage.

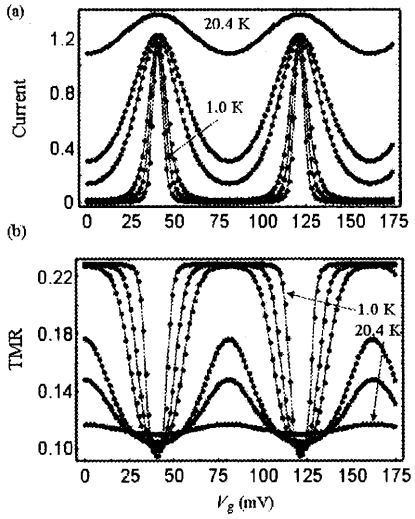

Fig. 6. (a) I-V_g and (b) corresponding TMR based on the same structure, and the same temperature range as in Fig. 5.

Hence, at $0.1T_0$ (10.2 K), the classic CB and gate oscillations are still clearly evident, whereas the TMR modulation has diminished by about 5-fold (e.g. 12.6% to 2.6% for the case of I-V_g), and has practically vanished at $0.2T_0$ (20.4 K). The fact that this low temperature threshold applies to the smallest island size of 10 nm (which is at the very limits of electron-beam lithography), points to the practical challenge of utilizing TMR modulation in a metallic double-junction circuit.

4. Conclusions

We have performed a precise capacitance calculations of a Ni-NiO-Ni double junction circuit coupled to a planar back gate. It is important to perform these calculations because important operational parameters such as the bias gate oscillations and operational temperature range are dependent on the gate C_g and island self-capacitance C_s, respectively. Our calculated values show a wide discrepancy from those obtained from commonly-used analytical formulae. This is especially so for C_s, where the analytical estimate yields a C_s value which is ~ 5 times smaller, and thus seriously overestimates the maximum operational temperature. Our capacitance analysis also suggests that an extended back gate covering both the island and contacts gives superior gate sensitivity, with minimal increase in C_s. Based on the precise capacitance values for the smallest island size w = 10 nm, we calculated the I-V and I-V_g based on the "orthodox" theory of single charge tunneling, complemented by higher-order cotunneling. We find that Coulomb gap and gate oscillation is thermally washed out at T ~ 30 K, while the spin-dependent phenomenon of TMR modulation diminishes rapidly at T beyond 10 K. This suggests a stringent temperature requirement for the operation of CB devices based on planar metallic double junctions. Since the temperature dependence is obtained based on the dimensions of fabricated devices, it will form a basis for comparison with actual experimental results.

Acknowledgements This work was partly supported by the National University of Singapore Grant No. R-263-000-216-112. One of the authors (M. B. A. J.) would like to thank the Yokohama National University for financial support.

References

1) T. Miyazaki and N. Tezuka, *J. Magn. Magn. Mater.*, **139**, L231 (1995).
2) See for a review: H. Grabert, M.H. Devoret (Eds.), Single Charge Tunneling, NATO ASI Ser. B, vol. 294 (Plenum Press, New York, 1992).
3) K. K. Likharev, *IBM J. Res. Dev.*, **32**, 144 (1988).
4) K. Majumdar and S. Hershfield, *Phys. Rev. B* **57**, 11521 (1998).
5) J. Barnas and A. Fert, *Phys. Rev. Lett.*, **80**, 1058 (1998).
6) K. Ono, H. Shimada and Y. Ootuka, *J. Phys. Soc. Japan*, **67**, 2852 (1998).
7) W. Kuo and C. D. Chen, *Phys. Rev. B* **65**, 104427 (2002).
8) M. Pirmann, J. v. Delft and G. Schön, *J. Magn. Magn. Mater.*, **219**, 104 (2000).
9) S. Takahashi and S. Maekawa, *Phys. Rev. Lett.*, **80**, 1758 (1998).
10) S. Mitani, S. Takahashi, K. Takanashi, K. Yakushiji, S. Maekawa, and H. Fujimori, *Phys. Rev. Lett.*, **81**, 2799 (1998).
11) T. Zhu and Y. J. Wang, *Phys. Rev. B*, **60**, 11918 (1999).
12) K. Yakushiji, S. Mitani, K. Takanashi, S. Takahashi, S. Maekawa, H. Imamura, and H. Fujimori, *Appl. Phys. Lett.*, **78**, 515 (2001).
13) Y. Takemura and J. Shirakashi, *Jpn. J. Appl. Phys. 1*, **40**, 128 (2001).
14) J. Shirakashi, K. Matsumoto, N. Miura, and M. Konagai, *Appl. Phys. Lett.*, **72**, 1893 (1998).
15) J. Shirakashi and Y. Takemura, paper 19pA-12, 27th Magnetic Society of Japan Conference, Osaka, 2003.
16) M. H. Devoret, D. Esteve, H. Grabert, G.-L. Ingold, H. Pothier, and C. Urbina, *Phys. Rev. Lett.*, **64**, 1824 (1990).
17) G.-L. Ingold and Y. V. Nazarov, in Ref. 2, Chap. 2, p. 21.
18) D. V. Averin and Y. V. Nazarov, *Phys. Rev. Lett.*, **65**, 2446 (1990).
19) K. Nabors and J. White, *IEEE Trans. Computer-Aided Design*, **10**, 1447 (1991).
20) K. Nabors, S. Kim, and J. White, *IEEE Trans. Microwave Theory Tech.*, **40**, 1496 (1992).
21) M. Julliere, Phys. Lett. 54A, 225 (1975).
22) D. V. Averin, *Physica B*, **194-196**, 979 (1994).
23) H. D. Jensen and J. M. Martinis, *Phys. Rev. B* **46**, 13407 (1992).
24) P. G. Hoel, C. J. Stone, and S. C. Port, Introduction to Stochastic Processes, p. 29 (Waveland, 1987).
25) A. Brataas, M. Hirano, J. Inoue, Yu. V. Nazarov, and G. E. W. Bauer, *Jpn. J. Appl. Phys.*, **40**, 2329 (2001).
26) R. Meservey and P.M. Tedrow, *Phys. Rep.*, **238**, 174 (1994).

Received Oct 20, 2003; Accepted Jan. 15, 2004.